Journal of Materials Chemistry A

RSC Publishing

PAPER

View Article Online
View Journal | View Issue

Cite this: J. Mater. Chem. A, 2013, 1, 10805

Anticorrosive conductive polyurethane multiwalled carbon nanotube nanocomposites

Huige Wei,[ab] Daowei Ding,[a] Suying Wei*[ab] and Zhanhu Guo*[a]

Conductive polyurethane (PU) nanocomposite coatings filled with multiwalled carbon nanotubes (MWNTs) fabricated by employing an *in situ* surface-initiated-polymerization (SIP) method were tested for corrosion prevention of stainless steel (SS). The nanocomposites exhibited a good response of electrical conductivity change to the strain during the cyclic tensile strain test. The anticorrosion properties of these nanocomposite coatings on the SS surface were evaluated in 3.0 wt% NaCl aqueous solution by monitoring the open circuit potential (E_{ocp}) and tracing quasi-stationary polarization (Tafel) of the nanocomposite-coated stainless steel (MWNT/PU–SS) electrode. Electrochemical impedance spectroscopy (EIS) was also obtained to give an insight into the anticorrosion protection of SS. The nanocomposite displayed a good chemical stability over long immersion in a corrosive environment. A significant positive shift of nearly 1.0 V in the E_{ocp} was observed from the E_{ocp}–time curve. Extrapolation of Tafel plots gave a much more positive corrosion potential (E_{corr}) and a lower corrosion current (I_{corr}). A protection efficiency as high as 97.70% was obtained. An equivalent circuit of the coating was proposed to fit the EIS data, confirming an effective corrosion protection for SS. The results indicate that the polyurethane matrix combined with the well dispersed MWNT reinforcements provided a significant physical barrier against the attack of corrosive ions in the solution for SS while providing a channel for the conductivity.

Received 18th May 2013
Accepted 5th July 2013

DOI: 10.1039/c3ta11966a

www.rsc.org/MaterialsA

1 Introduction

The corrosion of structural metals, *i.e.*, the alloys of iron and aluminum, usually involves the oxidation of metals and the reduction of oxygen, protons (H^+), and/or water.[1] As one of the most serious problems, corrosion imposes a major impact on the economics of industrial nations. Therefore, corrosion protection has become an issue of prime importance especially in the modern metallic finishing industry.[2] Varieties of strategies have been developed to control the dynamics of corrosion (slowing down the kinetics and/or altering the corrosion mechanism). Cathodic protection (employing a sacrificial anode or an external power supply) and anodic protection (maintaining a protective passive (oxide) layer on the metal surface) have been employed to decrease the oxidation or reduction rate, respectively.[3]

Recently, intrinsically conductive polymers (ICPs) including polyaniline (PANI),[4,5] polypyrrole (PPy),[6] polythiophene and their derivatives[7,8] have become a topic of current interest for corrosion prevention of metals.[9,10] These ICPs can be either used in their pure form[11] or composite forms,[12,13] primer coatings with conventional topcoat,[14] blended with conventional paints,[15] or additives to modify a conventional paint.[16] Different protection mechanisms have been proposed to explain the anticorrosion protection of ICPs. By studying anticorrosive PANI coatings on the steel substrate, Deberry[17] and Wessling[18] demonstrated that the anticorrosion protection can be achieved by an anodic protection mechanism, for example, the generation of an iron oxide layer (Fe_3O_4, α-Fe_2O_3 and γ-Fe_2O_3) with high protection ability at the interface of steel and PANI. The corrosion can be prevented by the generated electric field from the doped conducting polymers, which restricts the flow of electrons from metal to the outside oxidizing species, *i.e.*, oxygen.[19]

However, the difficult processability of ICPs used for anticorrosive purposes remains a challenge. The problem existing with these polymers prepared by chemical methods is that they are not easily melted and only slightly soluble in industrial solvents, and thus imposes lethal limitations on their applications for anticorrosive coatings.[19] Therefore, employing an electropolymerization technique to obtain a conductive polymer film directly on the metal substrate such as steel or aluminum has been adapted to deal with this issue. Unfortunately, there are also some problems remaining. One problem is that during the polymerization process, the dissolution of the metal substrates (or its passivation, metal oxide) occurs simultaneously due to the anodic polarization of the electrode. The

[a]Integrated Composites Laboratory (ICL), Dan F. Smith Department of Chemical Engineering, Lamar University, Beaumont, TX 77710, USA. E-mail: zhanhu.guo@lamar.edu; suying.wei@lamar.edu

[b]Department of Chemistry and Biochemistry, Lamar University, Beaumont, TX 77710, USA

polymer films cannot be obtained if the latter process is faster.[20] The other problem is the passivation of the metal, for example, Al_2O_3 is formed on Al by the galvanic interactions (a spontaneous oxidation–reduction process involving the dissolution of the metal anode and reduction of the cathode[21]) between the metal and the polymer. The formed oxides often act as a barrier and inhibit further electron transfer and monomer oxidation in the acidic solutions.[22]

Conventional organic coatings or paints, including epoxy, alkyd primers, and polyvinyl acetate and polyvinyl butyral, have also been used to protect metallic substrates from corrosion due to their low cost, easy application and aesthetic functionality.[23] It is generally accepted that the coatings provide a barrier blocking the passage of oxygen and water and increase the resistance of ion movement at the metal–electrolyte interface. In order to achieve reliable long-term anticorrosive performances, high loadings of inorganic pigments that release corrosion inhibiting substances are often added to the coatings. However, the toxic and carcinogenic nature of the inhibitors becomes a big concern for the environment and human health.[24] Thus, notable efforts have been made to replace the detrimental pigments.[25]

Polyurethane (PU) has been considered as one of the most versatile polymeric materials that are widely utilized as furniture, coatings, adhesives, constructional materials, fibers, padding, paints, elastomers and synthetic skins in the medical, automotive and industrial fields.[26,27] More research efforts have been focused on the study of magnetic properties,[28,29] or giant magnetoresistance behaviors[30] of polyurethane nanocomposites.

Since their discovery in 1991, carbon nanotubes (CNTs) have been intensely studied for a variety of scientific and technological applications due to their highly unique electronic, mechanical, catalytic, adsorption, and transport properties.[31] CNTs can be divided into single-walled carbon nanotubes (SWNTs) and multi-walled carbon nanotubes (MWNTs) based on the physical structure difference. Recently, the excellent mechanical properties of CNTs have made them applicable as reinforcements for structural materials.[32] However, employing conductive MWNT–PU composites for anticorrosion applications has rarely been reported.

In this work, the conductive polyurethane (PU) nanocomposites filled with 5.0 wt% multiwalled carbon nanotubes (MWNTs) were fabricated using an *in situ* surface-initiated-polymerization (SIP) method. The chemical structure and morphology of nanocomposites were studied using Fourier transform infrared spectroscopy (FT-IR) and scanning electron microscopy (SEM). The thermal stability and mechanical properties were investigated by thermogravimetric analysis (TGA) and tensile test, respectively. The *in situ* electrical conductivity in response to a cyclic strain of the composites was studied using a tensile test machine combined with a two-probe method. The anticorrosion performance of the MWNT–PU nanocomposite coating on the stainless steel (SS) substrate surface was evaluated in a 3.0 wt% NaCl aqueous solution by monitoring the open circuit potential (E_{ocp}) and tracing the quasi-stationary polarization (Tafel) of the coated SS electrode. Electrochemical impedance spectroscopy (EIS) was also conducted to obtain an insight into the process of the composite coating occurring in a corrosive environment. An equivalent circuit of the coating was proposed to fit the EIS data. The anticorrosion mechanism of the composite was also proposed based on the EIS plots of the MWNT–PU coated SS.

2 Experimental

2.1 Materials

Tetrahydrofuran (THF, 99%) was purchased from Fisher scientific. MWNTs (SWeNT SMW 200X, average diameter: 10.4 nm; average length: 4.3 μm) were provided by SouthWest NanoTechnologies, Inc. All the chemicals were used as received without any further treatment. The starting materials for the preparation of polyurethane were supplied by PRCDesoto international, Inc, containing three parts, A, B, and C. A (polyurethane STD-102, containing organotitanate) and C (a liquid containing aliphatic amine, parachlorobenzotrifluoride and methyl propyl ketone) are the accelerator and catalyst, respectively, and B is the two-part monomer (diol and diisocyanate). The monomers and the chemical reaction to yield polyurethane are shown in Scheme 1.

2.2 Fabrication of MWNT–PU nanocomposite coated-SS electrodes

The MWNT–PU nanocomposites were fabricated by the surface-initiated-polymerization (SIP) method. In the SIP method, both the accelerator A (0.36 g) and the catalyst C (0.40 g) were added to a MWNT suspended tetrahydrofuran solution (20.0 mL), which was followed by sonication for 1 h at room temperature to allow full adsorption of A and C on the MWNT surface. Then the two-part monomers (2.24 g) were introduced into the above solution to polymerize for 1 h at 50 °C. The suspension was observed to become more and more viscous as the reaction proceeded. The viscous solution prepared above was drop-cast onto a cylindrical stainless steel electrode with a geometric area of 17.68 mm^2 (diameter: 4.69 mm). The stainless steel was sanded with emery polishing paper and cleaned with ethanol before usage. The MWNT–PU coatings with a thickness of ~1 mm were also obtained by casting the solution onto a Si wafer. Both the electrodes and the thin films were put into a fume hood and kept at room temperature for additional seven days to ensure a complete reaction and solvent evaporation.

2.3 Characterization

2.3.1 Morphology and chemical structure determination. The morphology of the nanostructures was characterized with a scanning electron microscope (SEM, JEOL field emission scanning electron microscope, JSM-6700F).

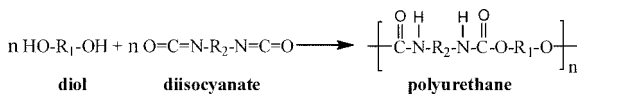

Scheme 1 Chemical formula of two-part monomers and the polymerization of polyurethane.

An FT-IR spectrometer coupled with an ATR accessory (Bruker Inc. Vector 22) was used to characterize the functionality of the MWNT–PU nanocomposites in the range of 500 to 4000 cm^{-1} at a resolution of 4 cm^{-1}.

2.3.2 Thermogravimetric analysis. The thermal stability of the MWNT–PU nanocomposites was studied with a thermogravimetric analysis (TGA, TA Instruments Q-500). The TGA was conducted from 25 to 800 °C with an air flow rate of 60 mL min^{-1} and a heating rate of 10 °C min^{-1}.

2.3.3 *In situ* conductivity in the cyclic strain of the MWNT–PU nanocomposite films. The *in situ* electrical conductivity during the cyclic strain test of the nanocomposite films was measured by combining the tensile test machine and a Keithley 2400 SourceMeter under voltage-source testing mode. Cyclic strain tests were carried out following the American Society for Testing and Materials (ASTM, D 882-Tensile Testing of Thin Plastic Sheeting) in a unidirectional tensile test machine (ADMET tensile strength testing system 2610) by applying a sawtooth force. The parameters (displacement and load) were controlled using a digital controller (MTESTQuattro) with MTESTQuattro®Materials Testing Software. The samples (thin films) were designed according to the ASTM standard requirement and prepared as described for the thin films. A crosshead speed of 500 mm min^{-1} was used and the strain (mm mm^{-1}) was calculated by dividing the jogging displacement by the original gauge length. All the samples were elongated to 186.0% first and the strain was controlled ranging from 186.0 to 192.0% during the stretching and recovery process. Scheme 2 illustrates the experimental set-up for the electrical conductivity measurement of the MWNT–PU nanocomposite films during the cycling strain tests. The nanocomposite film samples were fixed onto the tensile test machine, and then were covered with a piece of conductive copper tape (CU-35C, 3M) near both ends, respectively, and clamped by two electrodes (alligators) that were connected to the two outer probes of the Keithley 2400 SourceMeter. The voltage was set at 5.0 V and the corresponding current variation in the stretching and recovery processes was measured and recorded.

2.3.4 Anticorrosion behaviors of the MWNT–PU nanocomposite coating on stainless steel. The anticorrosive performance of the coating on stainless steel at different immersion times in the 3.0 wt% NaCl aqueous solution was evaluated on an electrochemical working station VersaSTAT 4 potentiostat (Princeton Applied Research). Scheme 3 represents a typical electrochemical cell consisting of a reference electrode, a working electrode, and a counter electrode. An Ag/AgCl electrode saturated with KCl served as the reference electrode and a platinum (Pt) wire as the counter electrode, respectively. Bare stainless steel (SS) or MWNT–PU nanocomposite coated stainless steel (MWNT/PU–SS) was sealed with cured epoxy resin so that only the bottom was in direct contact with the electrolyte and was used as the working electrode. To measure the open circuit potential, E_{ocp}, of the samples, a two-electrode system consisting of only the working electrode and the reference electrode was adapted. This potential may vary with time because of the changes occuring in the nature of the surface (oxidation, formation of the passive layer or immunity) of the electrode. After a period of immersion, the E_{ocp} was stabilized around a stationary value and then could be measured. In the case of Tafel polarization, the potential was scanned at ±200 mV *versus* the open circuit potential at a scan rate of 0.167 mV s^{-1}. From the anodic and cathodic polarization curves, the Tafel regions were identified and extrapolated to obtain the corrosion potential (E_{corr}) and the corrosion current (I_{corr}) using the General Purpose Electrochemical Software. Electrochemical impedance spectroscopy (EIS) was carried out in the frequency range from 100 000 to 0.01 Hz at a 10 mV amplitude referring to the open circuit potential. All the tests were conducted at room temperature.

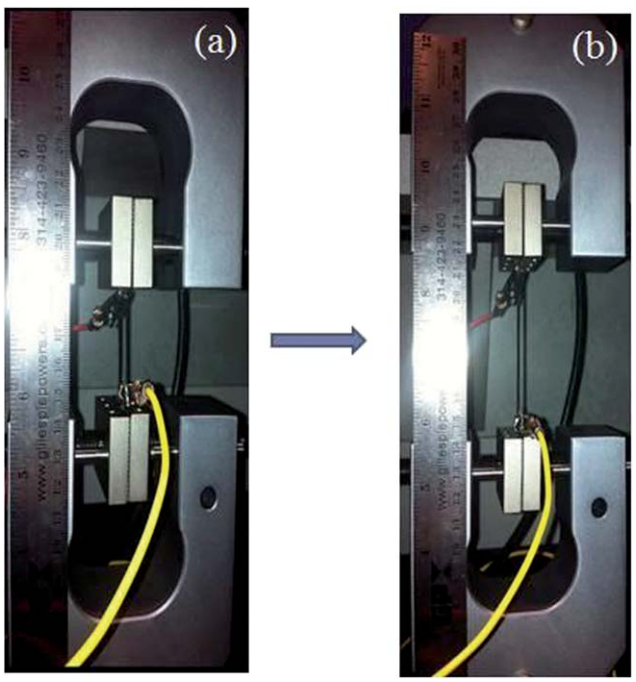

Scheme 2 Illustration of the experimental set up for *in situ* electrical conductivity measurement during the cyclic strain test. (a) and (b) show the composite film at different elongations during the stretching process.

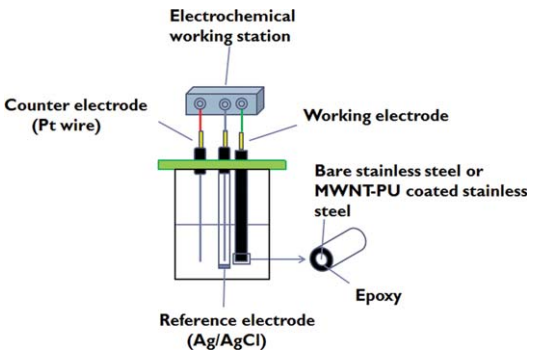

Scheme 3 Experimental configuration for the corrosion test.

3 Results and discussion

3.1 Morphology and chemical structure analysis

3.1.1 Morphology. Fig. 1 shows the morphology of pure PU and MWNT–PU composite films from a cross-sectional view. Pure PU, Fig. 1(a), displays a smooth structure. For the MWNT–PU nanocomposites, MWNTs are observed uniformly dispersed in the polymer matrix, and no phase separation occurred. In addition, the diameter of CNTs appears much bigger than their actual size, 10.4 nm. This phenomenon might be explained by the polymer growth surrounding the CNT walls, which in turn indicates a good compatibility between the MWNTs and the hosting polymer matrix.

3.1.2 FT-IR analysis. Fig. 2 shows the FT-IR spectra of the MWNTs, pure PU, and the MWNT–PU nanocomposites. MWNTs exhibit no characteristic absorbance peaks in the spectra, which are consistent with the reported few functional groups on the surface of the as-received MWNTs, and therefore all the characteristic peaks in the MWNT–PU nanocomposites mainly arise from the PU matrix. Besides the peaks at 2930 and 2850 cm^{-1} attributing to the vibration of –CH in $–CH_3$ and $–CH_2$, respectively, a broad peak at 3335 cm^{-1} corresponding to the –NH vibration[33] and an absorbance peak at 1550 cm^{-1} assigned to –CN[34] are observed in the spectra of the nanocomposites. The peaks at 1700, and 1237 cm^{-1} are due to the –C═O and –C–O stretching vibration, respectively.[35] No absorbance band around 2270 cm^{-1}, characteristic of the –NCO group in the diisocyanate monomer,[36] is observed, indicating a complete polymerization of the monomers during the curing of the MWNT–PU nanocomposites.

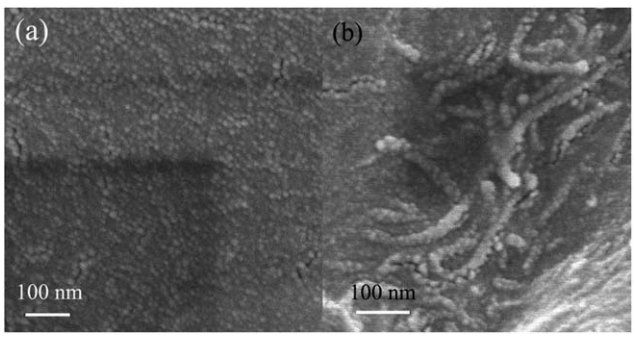

Fig. 1 SEM microstructures of the (a) pure PU and (b) MWNT–PU composite film from a cross-sectional view.

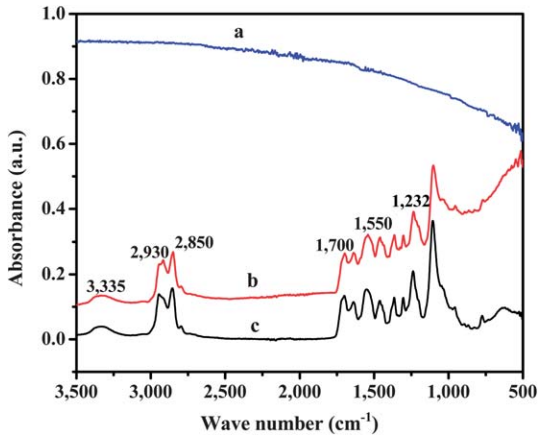

Fig. 2 FT-IR spectra of the (a) MWNTs, (b) MWNT–PU composites, and (c) pure PU films.

3.2 Thermal stability of the nanocomposites

The thermal stability of the pure PU and the MWNT–PU nanocomposites was studied by thermogravimetric analysis. Fig. 3 shows the weight percentage change of the material as a function of temperature. The addition of MWNTs made the polyurethane more stable with a higher complete decomposition temperature and little difference was observed in the onset decomposition temperature between the pure polyurethane and the composite. The pure polyurethane was decomposed completely at temperatures higher than 550 °C and the plateau level of the composites was attributed to the MWNT loading. When the MWNTs were added, the decomposition temperature was observed to be increased by 21 K. This is due to the retarding effect of the MWNTs on the movement of the polyurethane chains considering the inert nature of the MWNTs. This phenomenon has also been observed in the silicon carbide nanoparticle reinforced polyurethane[37] and the multiwalled carbon nanotube (MWNT) reinforced polybenzoxazine nanocomposites.[38]

3.3 *In situ* conductivity of the nanocomposites in the cyclic strain

The electrical conductivity of the nanocomposite was measured in the cyclic strain test. Fig. 4 shows the *in situ* resistance of the composite film in response to a cyclic strain test. The resistance of the nanocomposite film was observed to increase with increasing the strain generally. This phenomenon can be explained by two reasons. First, under the elongation condition, the length of the film increases and the cross-sectional area decreases, therefore the film displays an enlarged resistance as most conductive materials do. Second, the distance between the

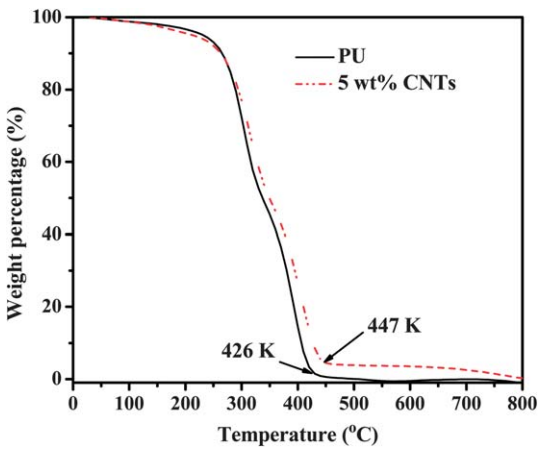

Fig. 3 TGA of the pure PU and the MWNT–PU nanocomposites.

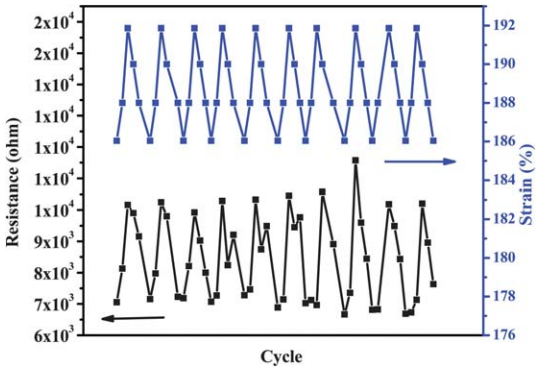

Fig. 4 *In situ* resistance of the MWNT–PU composite thin films in response to cyclic strain.

MWNTs dispersed in the hosting polymer becomes larger with increasing the strain and the contact among the MWNTs becomes poor during the stretching process, thus leading to an observed increased resistance. The good correlation between the resistance and the strain during the cyclic strain test renders the composites promising for strain sensors applications.[39]

3.4 Anticorrosion behaviors

The open circuit potential, E_{ocp}, indicates the thermodynamic tendency of a material to undergo electrochemical oxidation in a corrosive medium,[40] and it can serve as an indicator of cathodic protection of the coating. For example, active metals including aluminum or steel often give a negative E_{ocp}. For example, −0.6 V *versus* Ag/AgCl is reported for the uncoated steel and −0.78 V for the 2024 aluminum alloy and the E_{ocp} increases to around −0.5 and −0.25 V for the polyvinyl acetate coated steel[41] and Ce-coated aluminum,[42] respectively. Fig. 5 shows the E_{ocp} evolution of bare SS and MWNT/PU–SS as a function of immersion time in the 3.0 wt% NaCl solution, and Table 1 summarizes the E_{ocp} at different times. Different corrosion behaviors can be observed for bare SS and MWNT/PU–SS. For bare SS, the E_{ocp} is −973 mV after 10 h, and increases initially to around −700 mV, and then decreases to a lower value, and then rises again. The fluctuation of E_{ocp} can be explained by the fact that in the first stage of the corrosion process, passive metal oxides were formed at the electrode–electrolyte interface, as reported by Wessling,[43] and the E_{ocp} increased as a result of the cathodic protection by the metal oxides. The unstable metal oxides were gradually dissolved in the solution and the metallic surface was exposed to and attacked by the corrosive ions, leading to a decreased E_{ocp}. New passive layers were formed again and correspondingly the E_{ocp} was increased again. This conclusion can be verified by the red rust observed on the bare SS electrode in the beginning of the corrosion process and later the color change of the NaCl solution from colorless to yellow brown. A similar phenomenon has also been reported by Mrad *et al.* in stainless steel protected by the polyaniline film system.[44] Compared with bare SS, MWNT/PU–SS displays a much more enhanced E_{ocp}. An E_{ocp} of 11 mV after 10 h is obtained for MWNT/PU–SS, indicating that stainless steel is in the passive state and is well protected. The positive shift of E_{ocp} by nearly 1 V indicates better anticorrosive properties as compared to conductive films for anticorrosion applications (−860 to −870 mV for PPy/PANI bilayer conductive films in the E_{ocp}[45]). Besides, no drop in the E_{ocp} of the composite coated SS was observed during the test (50 mV after 360 h), confirming an intact protective coating by the MWNT–PU composites. The composites also exhibit fluctuations of E_{ocp}. Given the fact that there was no passive layer formed, as confirmed by the EIS study (section below), this phenomenon could not be caused by the interactions between the coating and the metal, which lead to the oxidation of metal occurring in the conductive polymer coated metal systems.[41,46] Instead, it is

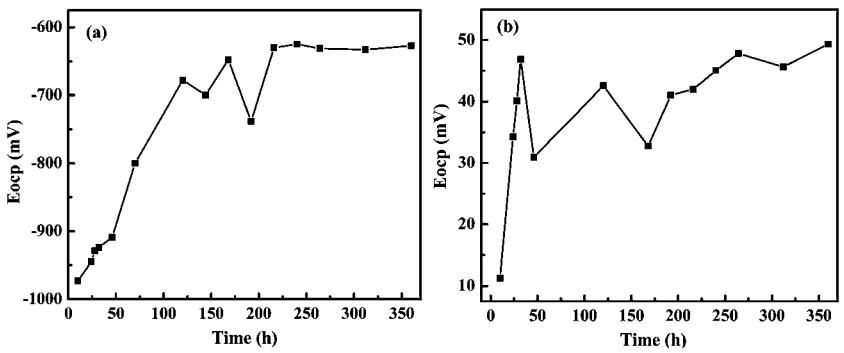

Fig. 5 The open circuit potential (E_{ocp})–time curves for (a) SS and (b) MWNT/PU–SS in 3.0 wt% NaCl solution.

Table 1 E_{ocp} of SS and MWNT/PU–SS at various exposure times in 3.0 wt% NaCl solution

Time (h)	10	24	28	32	46	120	168	192	216	240	264	312	360
SS	−973	−945	−929	−924	−909	−678	−648	−738	−630	−625	−631	−633	−627
MWNT/PU–SS	11	34	40	47	31	43	33	41	33	45	48	46	49

inferred that the fluctuation of the E_{ocp} in the nanocomposite coating originates from the low number of electrical contacts between MCNT particles, where a similar phenomenon was also observed in the zinc-rich anticorrosive coating.[47] Besides, in contrast to what happened for bare SS, no rust was formed on the MWNT/PU–SS electrode or color change occurred in the NaCl solution. Both the measurements and the visual observations confirm the excellent anticorrosive behaviors of the coating.

Corrosion rate can be obtained by the Tafel extrapolation method, where large cathodic and anodic polarizations provide the cathodic and anodic polarization curves for the respective corrosion processes.[48] Extrapolation of these curves in their linear regions to the point of intersection provides both the corrosion potential (E_{corr}) and the corrosion current (I_{corr}). The more negative E_{corr} and the larger I_{corr} usually correspond to faster corrosion rates while the more positive E_{corr} and the smaller I_{corr} mean a slower corrosion process.[49,50] Fig. 6 shows the typical Tafel curves of bare SS and MWNT/PU–SS at different immersion times in the 3.0 wt% NaCl solution, and Table 2 gives the E_{corr} and I_{corr} extrapolated from the Tafel curves. In the case of bare SS, the E_{corr} is −919 mV in the beginning, and initially shifted toward a positive position a little bit, and then decreased again. I_{corr} exhibits a similar trend to E_{corr}, implying the formation and later break-down of the passive (oxide) layers, which is in good agreement with the results of open current potential measurement. For the nanocomposite coated SS, a significantly positively shifted E_{corr} of −53 mV was obtained, confirming an effective corrosion protection by the coating. The E_{corr} did not change much over a long immersion time, indicating the good chemical stability of the nanocomposite coatings in a corrosive environment over a long immersion time. I_{corr} is also found to be decreased significantly from 286 nA for bare SS to 13.5 nA for the composite coated SS at 312 h, implying that the corrosion process is significantly reduced by the composite coating. The composite shows a more positive E_{corr} and three orders of magnitude decreased I_{corr} as compared to PANI coated stainless steel (around −0.57 V in the E_{corr} and ~1 μA in the I_{corr}),[51] implying much better corrosion protective properties of the MWNT–PU coating.

The corrosion rate (R_{corr}, mm per year) was calculated from eqn (1):[52]

$$R_{corr} = \frac{i_{corr} M}{DV} \times 3270 \quad (1)$$

where i_{corr} is the corrosion current density (corrosion current divided by the area of the electrode, A cm^{-2}), M is the molecular weight of the metal subjected to corrosion (g mol^{-1}), V is the valency (the number of electrons lost during the oxidation reaction of the metal, 2 for the oxidation of steel), 3270 is a constant ($3270 = 10 \times 1 \times 1\text{cm} \times \frac{10\text{mm}}{1\text{cm}}$ 1 year (in s)/96497.8 (C mol^{-1})),[53] and D is the density of the corroding metal (g cm^{-3}, 7.85 for stainless steel). The polarization resistance, or corrosion resistance,[41] R_p, (the slope of the polarization curve at the E_{corr}[54]) which is correlated with the corrosion rate, R_{corr}, was obtained from the Tafel plots according to the Stearn–Geary equation (2):[55]

$$R_p = \frac{b_a b_c}{2.303(b_a + b_c) i_{corr}} \quad (2)$$

where i_{corr} is the corrosion current (A cm^{-2}), b_a and b_c are the anodic and cathodic Tafel slopes ($\Delta E/\Delta \log i$, where large values of b_a and b_c correspond to faster reaction rates and are dependent on the temperature[56]), respectively. The protection efficiency (P_{EF}%) values were estimated using the eqn (3):[57]

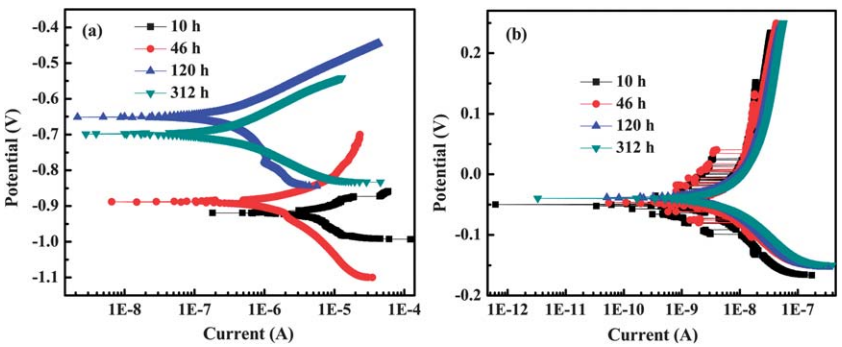

Fig. 6 Tafel curves of the (a) SS and (b) MWNT/PU–SS electrodes.

Table 2 E_{corr} and I_{corr} of SS and MWNT/PU–SS extrapolated from the fitting data of Tafel curves

	Time (h)	10	24	28	32	46	120	168	192	216	240	264	312
E_{corr}/mV	SS	−919	−939	−899	−880	−888	−763	−650	−682	−634	−671	−648	−698
	MWNT/PU–SS	−53	−60	−49	−46	−49	−47	−48	−37	−35	−31	−39	−44
I_{corr}/nA	SS	67 925	1862	3382	1208	2407	92	858	1151	289	449	188	286
	MWNT/PU–SS	4.4	3.8	10.6	3.5	5.7	11.0	9.6	11.1	11.0	12.2	13.0	13.5

$$P_{EF}\% = \frac{R_p^{-1}(\text{uncoated}) - R_p^{-1}(\text{coated})}{R_p^{-1}(\text{coated})} \times 100 \quad (3)$$

The electrochemical corrosion parameters obtained from the extrapolation of Tafel at 312 h for bare SS and MWNT–PU coated SS are given in Table 3.

As seen from Table 3, R_{corr} is calculated to be 1.885 and 0.089 mm per year for bare SS and the composite coated SS, respectively, using eqn (1). Therefore, it can be concluded that the corrosion rate is reduced greatly when the nanocomposite film is coated on SS. R_p is found to be 3.04×10^6 Ω for the nanocomposite coated SS, which is much higher than that of bare SS, 0.07×10^6 Ω for pure SS. The parameters clearly demonstrate a high corrosion resistance provided by the nanocomposite coating. A P_{EF}% as high as 97.70% is obtained for the nanocomposite coated SS, which is higher than the reported values, ~90% obtained in the polyaniline coatings on an aluminum alloy 3004 system.[22] The results from Tafel curves confirm that the nanocomposite film provides steel a dense barrier against the attack of the corrosive ions.

3.5 Anticorrosion mechanism

Stainless steel is subjected to corrosion by oxygen or water, which is illustrated by the following reactions:[58]

$$Fe \rightarrow Fe^{2+} + 2e^-$$

$$Fe^{2+} \rightarrow Fe^{3+} + e^-$$

$$O_2(g) + 2H_2O + 4e^- \rightarrow 4OH^-$$

$$4Fe^{2+}(aq) + O_2(g) + 6H_2O \rightarrow 4FeOOH + 8H^+$$

From the reactions, it can be concluded that H_2O and O_2 are necessary for the corrosion of steel. Effective corrosion prevention can be achieved if H_2O or O_2 is prevented from accessing the surface of the metal substrate. EIS is a powerful tool to study the corrosion protection mechanism of the coatings.[59] Fig. 7 represents the EIS of the MWNT–PU coated SS during different immersion times. No obvious increase in the resistance was observed for the electrode after 46 h, indicating that no metal oxides were formed at the stainless steel–composite interface. The composite coating serves as an effective physical barrier so that no corrosive ions in the electrolyte could penetrate across the coating to induce the corrosion of steel. An equivalent circuit, inset of Fig. 7, was proposed from the EIS data. The equivalent circuit consists of a capacitance of the coating (C_c, F), a pore resistance (R_p, Ω), which is considered to be due to the formation of ionically conducting paths in the polymer,[60] and a capacitance of the double layer at the electrode–electrolyte interface (electric charges accumulating on the electrode surfaces and ions of the opposite charge arranged in the electrolyte side, C_{dl}, F),[61] and a charge transfer resistance (R_{ct}, Ω). R_{ct} is a parameter of the resistance to electron transfer across a metal surface and is inversely proportional to the corrosion rate. A higher R_p implies a smaller number of H_2O and O_2 molecules diffused into the coating.[62] A uniform and defect-free coating usually displays a higher R_p and R_{ct}, and lower C_c and C_{dl}.[22] Table 4 gives the fitting parameter values from the equivalent circuit of the EIS obtained from 3.0 wt% NaCl aqueous solution. The observed higher values of R_p and R_{ct} and the lower values of C_c and C_{dl} imply that the nanocomposite coating offers an excellent corrosion protection to stainless steel. It can also be observed that R_p decreases with the prolongation of immersion time, which is reasonable as more and more corrosive species are diffusing into the coating. Interestingly, no passive layers are formed for the composite

Table 3 Electrochemical corrosion parameters for bare SS and MWNT–PU coated SS in 3.0 wt% NaCl solution

Electrodes	E_{corr} (mV)	i_{corr} (A cm^{-2})	b_a (mV)	b_c (mV)	R_p (Ω)	P_{EF}%
SS	−698.0	1.62×10^{-4}	105.97	82.64	7.06×10^4	—
PU/MWNT–SS	−43.6	7.63×10^{-6}	318.16	134.45	3.04×10^6	97.70

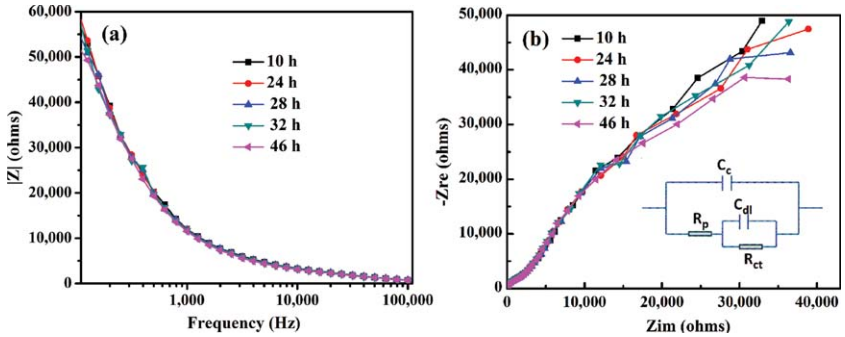

Fig. 7 EIS of the MWNT/PU–SS electrode. Inset is the equivalent circuit.

Table 4 Fitting parameter values from the equivalent circuit of the EIS obtained from 3.0 wt% NaCl aqueous solution

time (h)	R_p (Ω)	C_c (F)	C_{dl} (F)	R_{ct} (Ω)
10	4974	2.234×10^{-9}	1.346×10^{-8}	8.22×10^{4}
24	4709	2.352×10^{-9}	1.332×10^{-8}	7.751×10^{4}
28	4786	2.364×10^{-9}	1.337×10^{-8}	7.459×10^{4}
32	4641	2.405×10^{-9}	1.347×10^{-8}	7.735×10^{4}
46	4499	2.479×10^{-9}	1.365×10^{-8}	6.749×10^{4}

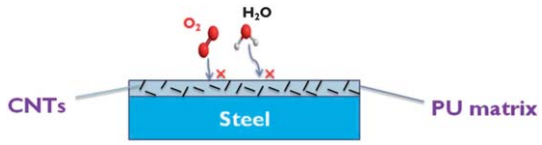

Scheme 4 Illustration of the anticorrosion mechanism of MWNT–PU composite coating.

coating protected-SS as suggested by the EIS data, indicating the excellent anticorrosive behavior of the nanocomposite coating.

Based on the information provided by EIS, Scheme 4 illustrates the anticorrosion mechanism of the conductive MWNT–PU coating. The presence of inorganic or organic fillers in the polymer matrix usually constitutes a solid barrier in the path of the gas molecules passing through the polymer.[52] A more tortuous path in the composite is imposed upon the gas molecules to penetrate into the polymeric matrix, and thus retarding the corrosion progress. The higher the aspect ratio of the filler, the larger the filler-matrix interfacial area, and the more tortuous the path, and thus the greater the decrease in the permeability will be.[63] The high aspect ratio (~1000 (ref. 64)) combined with the good dispersion of MWNTs in the polymer matrix is believed to be capable of reducing the permeability of the MWNT–PU coating significantly. With the diffusion of the corrosive species (dissolved oxygen and chloride ions) blocked, the cathodic reactions taking place across the metal–electrolyte interface can be inhibited correspondingly.

4 Conclusions

The conductive MWNT–PU nanocomposite coating was first studied for protecting stainless steel from corrosion in 3.0 wt% NaCl aqueous solution. MWNTs were observed to be uniformly dispersed in the PU matrix and the composite exhibits an enhanced thermal stability. *In situ* conductivity in the cycling strain test reveals the good response of electrical conductivity change to the strain during the cyclic tensile strain test. The effective anticorrosion behaviors of the composite coating were confirmed by a significant positive shift of nearly 1 V in the open current potential at the beginning of the corrosion process and remarkably reduced corrosion current (286 and 13.5 nA for bare SS and composite coated SS, respectively, after 312 h). A high protection efficiency of 97.70% is obtained for the composite coating. The nanocomposite coating also exhibits a good chemical stability in a corrosive environment with no degradation of the coating occurred over a long immersion time in the corrosive environment. An equivalent circuit of the coating was proposed to fit the EIS data, confirming an effective corrosion protection for stainless steel. The significant protection might be attributed to a solid barrier of the PU polymer matrix combined with the well-dispersed MWNTs, which increases the diffusion path of the corrosive ions, and thus renders the penetration of corrosive ions more difficult. The nanocomposite coatings show excellent corrosion inhibition properties and promise as anticorrosion materials in many applied fields.[65]

Acknowledgements

This project is financially supported by the Research Enhanced Grant of Lamar University.

References

1 D. A. Jones, *Principles and Prevention of Corrosion*, 1996.
2 D. E. Arthur, A. Jonathan, P. O. Ameh and C. Anya, *Int. J. Ind. Chem.*, 2013, **4**, 2.
3 D. E. Tallman, G. Spinks, A. Dominis and G. G. Wallace, *J. Solid State Electrochem.*, 2002, **6**, 73.
4 A. Özyılmaz and M. Erbil, *Curr. Appl. Phys.*, 2006, **6**, 1.
5 A. Olad, M. Barati and H. Shirmohammadi, *Prog. Org. Coat.*, 2011, **72**, 599.
6 D. M. Lenz, M. Delamar and C. A. Ferreira, *J. Electroanal. Chem.*, 2003, **540**, 35.
7 U. Rammelt, P. Nguyen and W. Plieth, *Electrochim. Acta*, 2001, **46**, 4251.
8 U. Rammelt, P. Nguyen and W. Plieth, *Electrochim. Acta*, 2003, **48**, 1257.
9 J. F. Rubinson, *ACS Symp. Ser.*, 2003, **832**, 2.
10 X. G. Li, M. R. Huang, W. Duan and Y. L. Yang, *Chem. Rev.*, 2002, **102**, 2925.
11 Y. Chen, X. Wang, J. Li, J. Lu and F. Wang, *Corros. Sci.*, 2007, **49**, 3052.
12 T. Tüken and M. Erbil, *Mater. Chem. Phys.*, 2006, **99**, 459.
13 M. Mahmoudian, W. Basirun, Y. Alias and A. Khorsand Zak, *Thin Solid Films*, 2011, **520**, 258.
14 M. Bagherzadeh, M. Ghasemi, F. Mahdavi and H. Shariatpanahi, *Prog. Org. Coat.*, 2011, **72**, 348.
15 G. Alvial, T. Matencio, B. R. A. Neves and G. G. Silva, *Electrochim. Acta*, 2004, **49**, 3507.
16 E. Armelin, C. Alemán and J. I. Iribarren, *Prog. Org. Coat.*, 2009, **65**, 88.
17 D. W. DeBerry, *J. Electrochem. Soc.*, 1985, **132**, 1022.
18 B. Wessling, *Synth. Met.*, 1997, **85**, 1313.
19 A. Baldissera and C. Ferreira, *Prog. Org. Coat.*, 2012, **75**, 241.
20 J. L. Camalet, J. C. Lacroix, T. D. Nguyen, S. Aeiyach, M. Pham, J. Petitjean and P. C. Lacaze, *J. Electroanal. Chem.*, 2000, **485**, 13.
21 Q. Liu, H. Li and L. Zhou, *Appl. Geochem.*, 2008, **23**, 2316.
22 M. Shabani-Nooshabadi, S. Ghoreishi and M. Behpour, *Electrochim. Acta*, 2009, **54**, 6989.

23 M. Bethencourt, F. Botana, M. Cano, R. Osuna and M. Marcos, *Prog. Org. Coat.*, 2003, **47**, 164.
24 E. Armelin, R. Oliver, F. Liesa, J. I. Iribarren, F. Estrany and C. Alemán, *Prog. Org. Coat.*, 2007, **59**, 46.
25 B. Del Amo, R. Romagnoli, C. Deyá and J. González, *Prog. Org. Coat.*, 2002, **45**, 389.
26 D. Chattopadhyay and K. Raju, *Prog. Polym. Sci.*, 2007, **32**, 352.
27 M. Song and D. Cai, *Polyurethane Nanocomposites by In situ Polymerization Approach and Their Properties*, Wiley-VCH, 2011, p. 169.
28 Z. Guo, S. Park, S. Wei, T. Pereira, M. Moldovan, A. B. Karki, D. P. Young and H. T. Hahn, *Nanotechnology*, 2007, **18**, 335704.
29 J. Zhu, S. Wei, I. Y. Lee, S. Park, J. Willis, N. Haldolaarachchige, D. P. Young, Z. Luo and Z. Guo, *RSC Adv.*, 2012, **2**, 1136.
30 Z. Guo, S. Park, H. T. Hahn, S. Wei, M. Moldovan, A. B. Karki and D. P. Young, *Appl. Phys. Lett.*, 2007, **90**, 053111.
31 M. Meyyappan, *Carbon nanotubes: science and applications*, CRC, 2004.
32 H. Gu, S. Tadakamalla, X. Zhang, Y. Huang, Y. Jiang, H. A. Colorado, Z. Luo, S. Wei and Z. Guo, *J. Mater. Chem. C*, 2013, **1**, 729.
33 B. G. Zanetti-Ramos, E. Lemos-Senna, V. Soldi, R. Borsali, E. Cloutet and H. Cramail, *Polymer*, 2006, **47**, 8080.
34 S. Zhang, Z. Ren, S. He, Y. Zhu and C. Zhu, *Spectrochim. Acta, Part A*, 2007, **66**, 188.
35 B. Yang, W. Huang, C. Li and L. Li, *Polymer*, 2006, **47**, 1348.
36 S. S. Narine, X. Kong, L. Bouzidi and P. Sporns, *J. Am. Oil Chem. Soc.*, 2007, **84**, 65.
37 Z. Guo, T. Y. Kim, K. Lei, T. Pereira, J. G. Sugar and H. T. Hahn, *Compos. Sci. Technol.*, 2008, **68**, 164.
38 Q. Chen, R. Xu and D. Yu, *Polymer*, 2006, **47**, 7711.
39 J. Zhu, S. Wei, J. Ryu and Z. Guo, *J. Phys. Chem. C*, 2011, **115**, 13215.
40 A. A. H. Kadhum, A. B. Mohamad, H. D. Jaffar, S. S. Yan and J. Hilo, *Int. J. Electrochem. Sci.*, 2013, **8**, 4571.
41 A. Adhikari, P. Claesson, J. Pan, C. Leygraf, A. Dédinaité and E. Blomberg, *Electrochim. Acta*, 2008, **53**, 4239.
42 X. Yu and C. Cao, *Thin Solid Films*, 2003, **423**, 252.
43 B. Wessling, *Adv. Mater.*, 1994, **6**, 226.
44 M. Mrad, L. Dhouibi and E. Triki, *Synth. Met.*, 2009, **159**, 1903.
45 C. Tan and D. Blackwood, *Corros. Sci.*, 2003, **45**, 545.
46 G. M. Spinks, A. J. Dominis, G. G. Wallace and D. E. Tallman, *J. Solid State Electrochem.*, 2002, **6**, 85.
47 A. Meroufel, C. Deslouis and S. Touzain, *Electrochim. Acta*, 2008, **53**, 2331.
48 N. Perez, *Electrochemistry and corrosion science*, Springer, 2004.
49 M. Yue, J. Zhang, W. Liu and G. Wang, *J. Magn. Magn. Mater.*, 2004, **271**, 364.
50 A. L. Rudd, C. B. Breslin and F. Mansfeld, *Corros. Sci.*, 2000, **42**, 275.
51 B. Grgur, M. Gvozdenović, V. Mišković-Stanković and Z. Kačarević-Popović, *Prog. Org. Coat.*, 2006, **56**, 214.
52 C. J. Weng, J. Y. Huang, K. Y. Huang, Y. S. Jhuo, M. H. Tsai and J. M. Yeh, *Electrochim. Acta*, 2010, **55**, 8430.
53 J. M. Yeh, H. Y. Huang, C. L. Chen, W. F. Su and Y. H. Yu, *Surf. Coat. Technol.*, 2006, **200**, 2753.
54 F. Mansfeld, *J. Solid State Electrochem.*, 2009, **13**, 515.
55 M. Stern and A. L. Geary, *J. Electrochem. Soc.*, 1957, **104**, 56.
56 A. J. Bard and L. R. Faulkner, *Electrochemical methods: fundamentals and applications*, Wiley, New York, 1980.
57 J. O. M. Bockris and A. K. Reddy, *Modern electrochemistry: an introduction to an interdisciplinary area*, Plenum Publishing Corporation, 1973.
58 C. H. Chang, T. C. Huang, C. W. Peng, T. C. Yeh, H. I. Lu, W. I. Hung, C. J. Weng, T. I. Yang and J. M. Yeh, *Carbon*, 2012, **50**, 5044.
59 C. Liu, Q. Bi and A. Matthews, *Corros. Sci.*, 2001, **43**, 1953.
60 G. Grundmeier, W. Schmidt and M. Stratmann, *Electrochim. Acta*, 2000, **45**, 2515.
61 W. Xing, S. Qiao, R. Ding, F. Li, G. Lu, Z. Yan and H. Cheng, *Carbon*, 2006, **44**, 216.
62 Y. Zhang, Y. Shao, T. Zhang, G. Meng and F. Wang, *Prog. Org. Coat.*, 2013, **76**, 804.
63 S. Sinha Ray, K. Yamada, M. Okamoto, A. Ogami and K. Ueda, *Chem. Mater.*, 2003, **15**, 1456.
64 B. I. Yakobson and P. Avouris, in *Carbon Nanotubes*, Springer, 2001, p. 287.
65 P. Marcus, *Corrosion mechanisms in theory and practice*, CRC Press LLC, 2011.